Journal of Intelligent Material Systems and Structures

*Original Article*

*Journal of Intelligent Material Systems and Structures*
2016, Vol. 27(11) 1461–1475

DOI: 10.1177/1045389X15595292
jim.sagepub.com
SAGE

# An optimized cross-linked network model to simulate the linear elastic material response of a smart polymer

**Jinjun Zhang[1], Bonsung Koo[1], Nithya Subramanian[1], Yingtao Liu[2] and Aditi Chattopadhyay[1]**

**Abstract**

This article presents a novel approach to model the mechanical response of smart polymeric materials. A cyclobutane-based mechanophore, named "smart particle" in this article, is embedded in an epoxy polymer matrix to form the self-sensing smart material. A spring–bead model is developed based on the results from molecular dynamics simulation at the nanoscale to represent bond clusters of a smart polymer. The spring–bead network model is developed through parametric studies and mechanical equivalence optimization to represent the microstructure of the material. A statistical network model is introduced, which is capable of bridging the high-accuracy molecular dynamics model at the nanoscale and the computationally efficient finite element model at the macroscale. A comparison between experimental and simulation results shows that the multiscale model can capture global mechanical response and local material properties.

**Keywords**

Multiscale modeling, spring–bead-based network model, molecular dynamics, optimization

## Introduction

Interest in stimuli-responsive materials that exhibit specific chemical reactions upon external stimuli such as temperature, pH, ion, light, and electric field has increased significantly in the last decade (Bawa et al., 2009; Qiu and Park, 2001; Richter et al., 2008; Suzuki et al., 1996; Tanaka et al., 1982). Particularly of interest are stress-sensitive materials responsive to mechanical loading (also known as mechanophores), which open novel ways to study post-yield behavior at the material level (Chang and Chang, 1987; Thostenson and Chou, 2006; Wu et al., 2008). Cho et al. (2010) and Chung et al. (2004) developed a cyclobutane-based mechanophore consisting of carbon–carbon covalent bonds. Under mechanical loading, the cyclobutane transforms into cinnamate groups, which emit green fluorescence. The cyclobutane-based mechanophore is embedded in an epoxy-based polymer matrix to form the self-sensing smart material. Previous studies have reported the experimental characterization and fabrication of nanoparticle-embedded polymers (Gibson, 2010). However, the determination of mechanical properties through testing is labor intensive and expensive. Several modeling techniques have also been developed to understand the nano- and microscale phenomena (Borodin et al., 2005; Fermeglia and Pricl, 2007; Ghosh et al., 1995) in hierarchical materials. These models provide important constitutive formulations and are a key to understanding the material response at the nano- and microscale.

To model polymeric systems integrated with nanoparticles, numerous approaches have been developed. These include homogenization techniques, molecular dynamics (MD) simulation, Monte Carlo (MC) simulation, and the Mori–Tanaka approach. In the epoxy-based polymer, the bonds (cross-linking) between the resin and the hardener molecules generate a large network structure. The heterogeneous cross-linking degree, which is defined as the percentage of actual cross-linked covalent bonds over all potential cross-linked bonds, has an important effect on the local mechanical properties (Fan and Yuen, 2007; Flory and Rehner, 2004; Krumova et al., 2000). In the last decade, a large

[1]School for Engineering of Matter, Transport & Energy, Arizona State University, Tempe, AZ, USA
[2]School of Aerospace and Mechanical Engineering, University of Oklahoma, Norman, OK, USA

**Corresponding author:**
Jinjun Zhang, School for Engineering of Matter, Transport & Energy, Arizona State University, Tempe, AZ 85287, USA.
Email: jzhan134@asu.edu

number of MD simulations on epoxy-based systems have been reported to understand material behavior at the molecular level (Hossain et al., 2010; Varshney et al., 2008). Yarovsky and Evans (2002) investigated the strength and molecular mechanisms of adhesion between an inorganic substrate and a cured epoxy resin using MD simulation. A method was presented in their work to predict cross-link density in the resin and curing agent molecules. Fan and Yuen (2007) conducted molecular level simulations to estimate the material properties of the cross-linked epoxy resin compound. Their work predicted the glass transition temperature ($T_g$), linear thermal expansion coefficients, and Young's modulus of the cross-linked epoxy resin compound.

The high computational cost associated with large-scale MD simulations limits its use beyond the nanoscale whereas the use of micromechanical homogenization techniques in a multiscale framework can lead to the propagation of large errors across length scales. Therefore, efforts have been made to maximize computational efficiency and maintain high accuracy while investigating the material behavior of polymers at the microscale. Techniques that rely on discrete material distribution and simplified analyses have been developed (Buxton and Balazs, 2002; Iwata, 2003; Schwarz et al., 2006). Underhill and Doyle (2005) developed a spring–bead model in which each bead represents a large segment of molecular chains, to model the mechanical response of a polymer. Furthermore, Gao et al. (2007) applied the spring–bead model to create a network model that can simulate larger polymer chains and microstructures; the network model was found to be more accurate than micromechanical approximation techniques for characterizing amorphous materials.

A review of multiscale modeling approaches for polymer nanocomposites has been presented by Zeng et al. (2008). The authors review simulation techniques such as MD and MC at the atomistic scale; Brownian dynamics, dissipative particle dynamics, and dynamic density functional theory method at the microscale; and equivalent continuum approach and finite element analysis (FEA) at the macroscale (Lin et al., 2012a, 2012b; Neerukatti et al., 2014; Peng et al., 2013). A major challenge is how to scale material behavior from the nano- and microscale to the macroscale in order to investigate the effect of the smart material at the structural scale. Despite the accuracy of MD simulations, computational inefficiency prohibits their use within a multiscale analysis framework. Recently, a multiscale analysis approach was employed to investigate the effect of carbon nanotubes (CNTs) embedded in polymer matrix for aerospace structural applications (Hasan et al., 2014). The composite cylinder assemblage method and the Mori–Tanaka theory were used to compute effective properties at the nanoscale and the microscale, respectively; the information served as inputs to the macroscale FEA of composite stiffeners. Although this was an important step toward integration of the relevant length scales within a multiscale framework, the methodology is not capable of capturing the interactions at the atomistic scale.

This article presents a spring–bead model and a network model which are developed to bridge nanoscale information to higher length scales for modeling epoxy polymers embedded with smart particles. Because mechanical properties are determined by inter/intramolecular potential energy and there is no reported literature on the mechanical properties of the smart polymer, MD simulation is the most appropriate approach to understanding the material properties of the smart polymer at the nanoscale. A series of MD simulations are performed to capture the generation of cross-linked bonds in the smart polymer; this information is further used to construct the probability distribution of cross-linking degrees. At the microscale, the material is partitioned into discrete mass beads which are linked using linear springs. By integrating multiple spring–bead models, a network model is generated to represent the elastic material properties. The experiments are conducted to validate the mechanical response predicted by the multiscale model. The developed methodology is computationally efficient and provides a possible means to bridge various length scales without significant loss of accuracy.

## Spring–bead model to represent bond clusters of polymer at the nanoscale

Micromechanical techniques allow the mechanical behavior of polymers to be understood through the continuum approximation of heterogeneous microstructures. The variation in microstructural properties leads to variable macroscopic properties. Because the mechanical behavior in nanocomposites is affected more by discrete phenomena, the application of continuum mechanics is not a suitable option at the microscale. The FE method and spring–bead-based method are the most widely used numerical methods for discretizing the continuum mechanical description of a material (Buxton and Balazs, 2002). The FE method incorporates a complex preprocessed mesh which allows detailed investigations of complex geometries at hot spots, while enabling complex constitutive relations to be incorporated. However, the accuracy and efficiency of FE method are dependent on mesh sizes, and therefore limitations exist on the level of complexity that can be simulated (Tomar et al., 2004). In order to simulate more heterogeneous microstructures, new technique may be adopted. The spring–bead model is considered as a two-dimensional (2D) or three-dimensional network of interconnecting one-dimensional linear springs. The continuous material is

lumped into discrete beads. The neighbor springs are linked together by the nodes fastened in the centers of the beads. The principal advantages of the model are the ease with which the microstructural heterogeneity can be incorporated through the local variation in spring characteristics and the simulation of crack propagation through the iterative removal of springs.

In this work, a spring–bead model is developed to characterize the elastic deformation of a cross-linked cluster of polymer chains with inputs from MD simulations that define local material properties. It should be clarified the spring–bead model is different from the traditional Rouse bead–spring model (Rouse and Prince, 1953). In this developed network model, the springs and beads are used as components in the cross-linked network. Springs are cross-linked to represent mechanical behavior of the material and bridge MD model and FEA model. The beads represent material mass of cluster bonds. Each spring is used to represent a cluster of polymer chains, instead of part of a single polymer chain. This simplification allows to bridge different models at multiple length scales and improves the simulation efficiency significantly. At each iteration step in the simulation, forces in the springs are applied to the nodes at the center of the beads, and the equilibrated nodal displacements throughout the system are calculated. Different from the traditional FE method for obtaining stress and strain, the spring–bead model provides the displacements of the nodes and forces in the springs. The equivalent strain and strain energy of spring–bead based network model can be defined and calculated using the displacements of nodes and the spring characteristics. Furthermore, the results from the network model can be scaled up to obtain the structural response at the macroscale using FEA (see Figure 1).

In this spring–bead model, each of the two beads serves as half of the mass of the bond cluster; the linear spring is used to represent the mechanical response (tensile and compressive) of the bond cluster, and the potential energy stored in the spring due to extension or compression captures the elastic strain energy in the deformed material. Variable spring stiffness (ratios of force to relative displacement) is used to represent bond clusters with different cross-linking degrees. It should be noted that the definition of this spring–bead model is dependent on the size of the bond cluster. To represent a bond cluster with a larger size, the mass of beads will be increased, and the spring stiffness will be increased as well. The linear relation between force and relative displacement can be expressed in equation (1)

$$F = k \cdot \Delta u \tag{1}$$

where $F$ is the attractive/repulsive force in the spring, $\Delta u$ is the relative displacement of the two beads compared to their original state, and $k$ represents the spring stiffness. The elastic energy stored in the spring can be expressed as

$$E = \frac{1}{2} \cdot k \cdot (\Delta u)^2 \tag{2}$$

where $E$ is the elastic energy stored in the spring. The elastic energy is used to calculate the equivalent strain energy density of the network model. However, the spring–bead model can only carry load in the uniaxial direction of the spring. At each point in the amorphous polymer material, there should be tensile, compressive, and shear load-carrying ability in all directions. Therefore, it is important that the network model with cross-linked springs and beads accurately represents the load-carrying capacity in all directions.

The existing setup of the spring–bead model can be extended to characterize the elastic–plastic material behavior by replacing the linear springs with

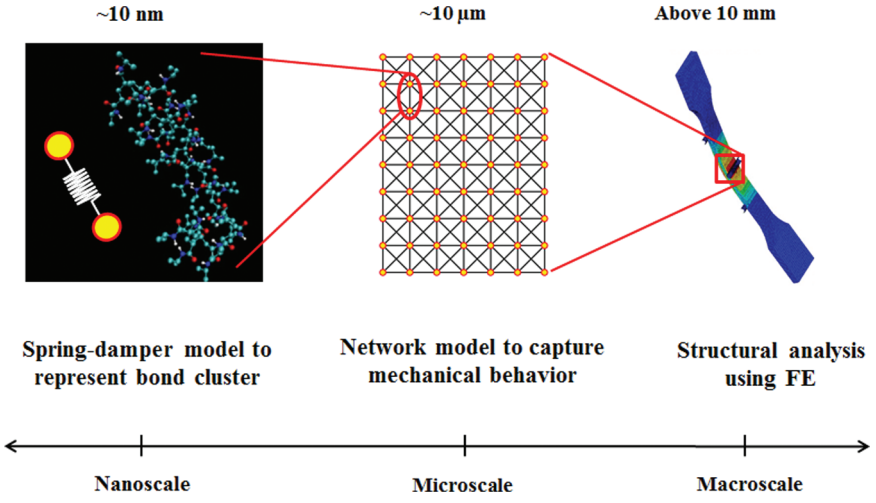


**Figure 1.** Modeling of polymer materials at the nanoscale, microscale, and macroscale.

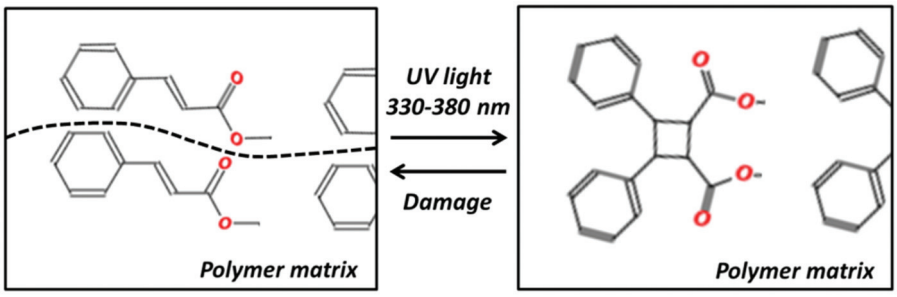


**Figure 2.** Schematic of UV-initiated cyclobutane generation and damage-induced cinnamoyl group generation.

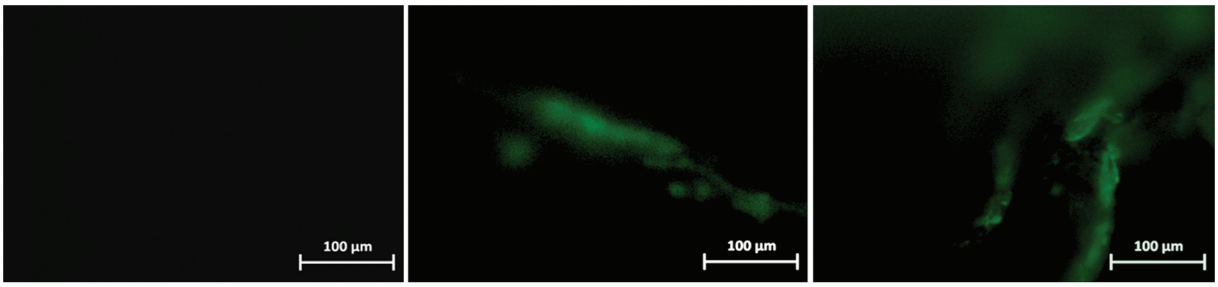


**Figure 3.** Fluorescence observation of smart polymer with increasing load: (a) no crack and no fluorescence observation, (b) micro crack and slight florescence intensity, and (c) major crack and higher florescence intensity.

appropriate nonlinear ones. Dampers can also be added in the spring–bead model to represent the nonlinear and viscoelastic properties of some materials. However, experimental tensile tests on the smart polymer material in this research record brittle behavior. There is no obvious plasticity region observed from these experimental tensile tests. Therefore, the spring–bead model and the subsequent network model developed in this study use linear springs to capture the mechanical response of the smart polymer. To construct a spring–bead model that can represent various cross-linking degrees at the molecular level, MD simulation is needed to obtain two important features of the material: statistical distribution of cross-linking degree and corresponding mechanical properties.

## MD simulation results to construct spring–bead model at the nanoscale

### *MD simulation of cross-linked bond clusters*

MD simulation is used to characterize the mechanical response of this smart polymer at the molecular level. A stochastic approach is used to estimate the most likely cross-linking degree of the polymer system. Some relevant research efforts (Bandyopadhyay et al., 2011; Li and Strachan, 2010; Tack and Ford, 2008) estimated the cross-linking degree indirectly by comparing the $T_g$ obtained from MD simulations and from differential scanning calorimetry (DSC). In this study, a direct approach to estimate the local cross-linking degree is introduced; this direct method mimics the experimental curing process using inter/intra-molecular potentials. The inter/intra-molecular potentials are determined by a force field, which is a set of functions and parameters achieved from experimental or quantum mechanical studies to describe material properties at the molecular level. The Merck molecular force field (MMFF) developed for general organic molecules is used for this study. The MD simulations are performed using the large-scale atomic molecular massively parallel simulator (LAMMPS) package (Plimpton et al., 2007).

The smart material used in this work comprises tris-(cinnamoyloxymethyl)-ethane (TCE) monomer to synthesize cyclobutane—a mechanophore formed by exposing the TCE monomer to ultraviolet (UV) light (wavelengths of range 330–380 nm), as shown in Figure 2. With local damage, the physical discontinuities break the covalent bonds in cyclobutane. Subsequently, the cyclobutane transforms into the TCE monomer, which consists of cinnamoyl groups that emit visible light of wavelengths ranging from 450 to 600 nm under UV excitation (Cho et al., 2008, 2010; Chung et al., 2004). Figure 3 shows the results observed from a uniaxial loading test. The UV fluorescence images were taken at different stages of the loading. There is no fluorescence observed in the elastic range of the smart polymer (see Figure 3(a)); slight fluorescence

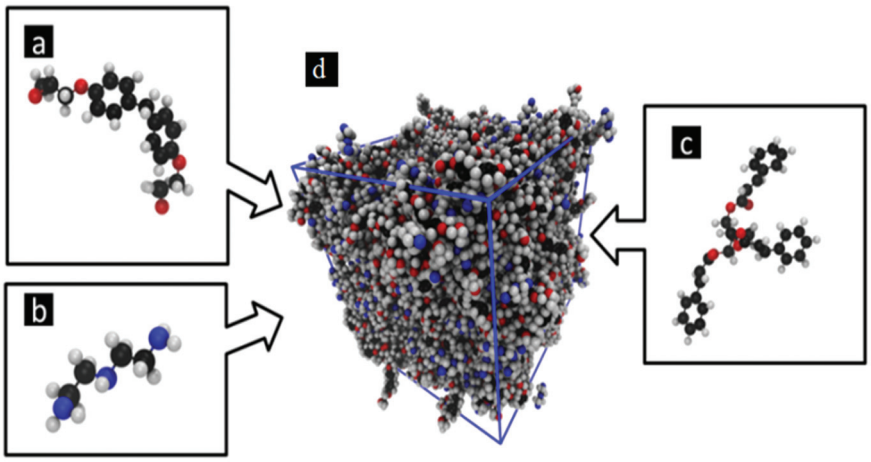


**Figure 4.** Components of smart polymer: (a) epoxy resin, (b) hardener, (c) smart material to form, and (d) RVE model.

**Table 1.** Components in the smart polymer.

| | Formula | Weight (g/mol) | Molecule number in one RVE |
|---|---|---|---|
| DGEBF | $C_{19}H_{20}O_4$ | 313 | 650 |
| DETA | $C_4H_{13}N_3$ | 103 | 550 |
| TCE | $C_{32}H_{30}O_6$ | 510 | 50 |

RVE: representative volume element; DGEBF: di-glycidyl ether of bisphenol F; DETA: di-ethylene tri-amine; TCE: tris-(cinnamoyloxymethyl)-ethane.

can be observed when micro cracks initiate in the specimen (Figure 3(b)). The intensity of the fluorescence keeps increasing with the growth of the micro cracks (Figure 3(c)). This observation provides evidence that the mechanophoric smart material is capable of capturing various levels of damage progression. MD simulation is adopted to further understand the interactions between the epoxy/hardener and the smart material, which could affect the color changing phenomena and the mechanical properties significantly.

### *Statistical cross-linking degree in MD simulation*

The molecular structures of the epoxy resin and the hardener that form the polymer used in this study are di-glycidyl ether of bisphenol F (DGEBF) and di-ethylene tri-amine (DETA), respectively (see Figure 4(a) and (b)). To simulate the variability in the cross-linking degree and the mechanical properties of the polymer system, a stochastic approach is proposed; a representative volume element (RVE) is constructed with molecules (of the resin, the hardener, and the smart particle) distributed randomly in the initial configuration (Figure 4(d)). The weight percentages of the components in this smart polymer are 70.9% for DGEBF, 19.1% for DETA, and 10.0% for TCE. Table 1 shows the respective chemical formulae, weights, and numbers of component molecules.

The epoxy-based polymer is an extensively cross-linked structure; additionally, the extent of cross-linking significantly affects the mechanical properties. A schematic epoxy network structure is shown in Figure 5 based on covalent bonds (represented by a black solid line in Figure 5(c)). The ellipse R (Figure 5(a)) and the circle H (Figure 5(b)) represent the epoxy resin and hardener, respectively. For epoxy resin particles, there are two active sites (Figure 5(a)), and for hardener particles there are five active sites (Figure 5(b)). A covalent bond will be generated when the distance between the active sites of the epoxy resin and the hardener is shorter than a critical value. The two active sites can share their electrons to stabilize the potential energy. The process of bond formation between the epoxy resin and the hardener molecules is also known as "curing" in polymer science.

A total of 500 MD simulations were performed, each with a randomly generated initial configuration (42,350 atoms in each RVE, 14 nm $\times$ 14 nm $\times$ 14 nm). After the initial configuration, an energy minimization based on the conjugate gradient algorithm is performed to avoid undesired repulsive forces between atoms. Periodic boundary conditions (PBCs) were applied to the boundaries of the RVE. Next, the isobaric–isothermal (NPT) ensemble simulation is conducted to equilibrate the RVE at standard room conditions (300 K and 1 atm) for 150 ps, which makes all the molecules grouped under the van der Waals and Coulomb interactions. Each RVE was cured using a bond formation command in LAMMPS and a cross-linking cut-off radius of 4.0 Å; this cut-off radius was selected because it is more than twice the length of a carbon–nitrogen covalent bond (Varshney et al., 2008; Yu et al., 2009). The resulting cross-linking degree is different for each RVE due to the random initial configuration. The frequency distribution of resulting cross-linking degrees (Figure 6) from the 500 MD

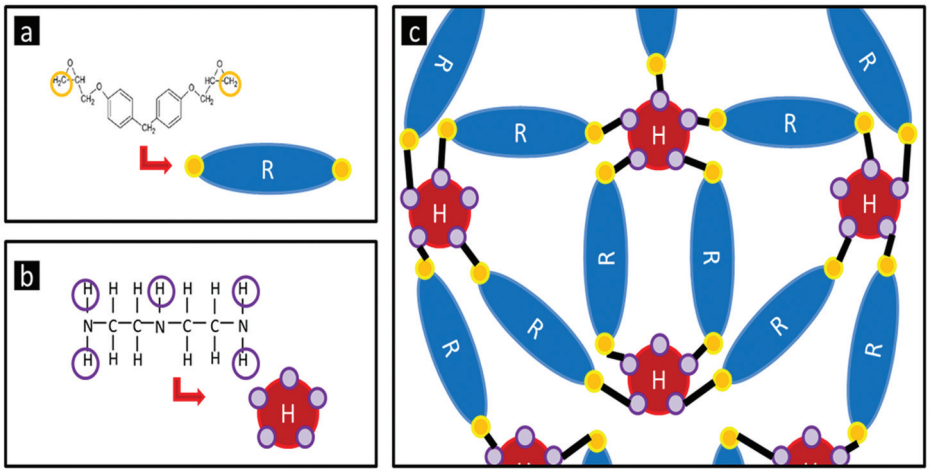


**Figure 5.** Schematic of cross-linked structure of epoxy resin and hardener: (a) molecular structure of epoxy resin with two active sites, (b) hardener with five active sites, and (c) epoxy resin and hardener are cross-linked to generate polymer structure. Black solid lines represent covalent bonds.

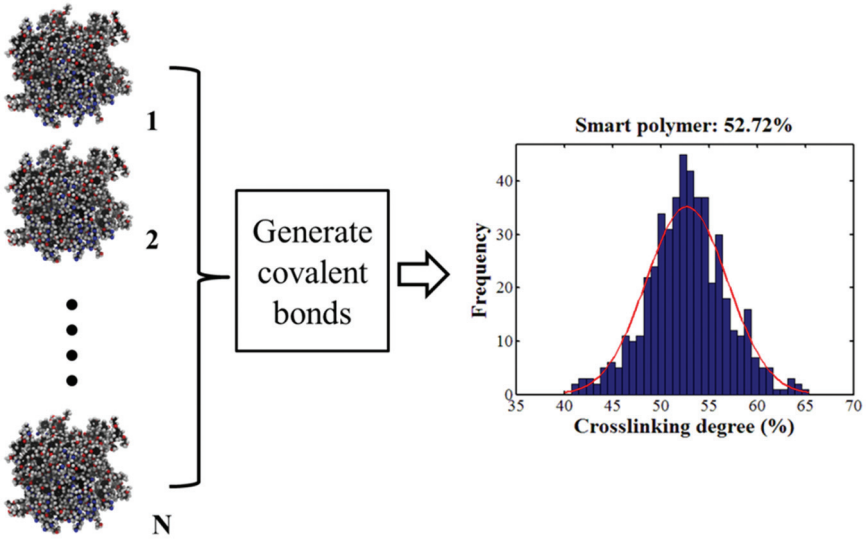


**Figure 6.** Statistical distribution of crossing-linking degrees based on MD simulations (N = 500).

simulations is statistically smooth. The simulation results indicate a quasi-normal distribution with cross-linking degrees ranging between 40% and 65%. The average cross-linking degree is 52.72% for the polymer system containing the smart material. These results are used to construct the statistical network model at the microscale.

## *Mechanical properties of smart polymer in MD simulation*

MD simulations were further performed on the cross-linked polymeric systems to obtain the tensile, compressive, and shear moduli. Uniaxial tensile/compressive tests were simulated on the atomistic systems with different cross-linking degree from 30% to 70%. The resulting RVEs with different cross-linking degrees were equilibrated at zero-atmospheric pressure to relieve residual stresses. The equilibrated RVEs were deformed along $x$-, $y$-, and $z$-axes independently under the NPT ensemble (300 K and 0 atm on the other axes). Based on the MD simulation result, Young's modulus of the polymer system is calculated in the elastic region. To determine the bulk modulus, triaxial deformation tests were simulated. The hydrostatic pressure on each RVE was varied from 0 to 5000 atm at room temperature; the change in volume was measured to obtain the bulk modulus based on equation (3)

$$K = \frac{\Delta p}{\Delta V / V_0} \tag{3}$$

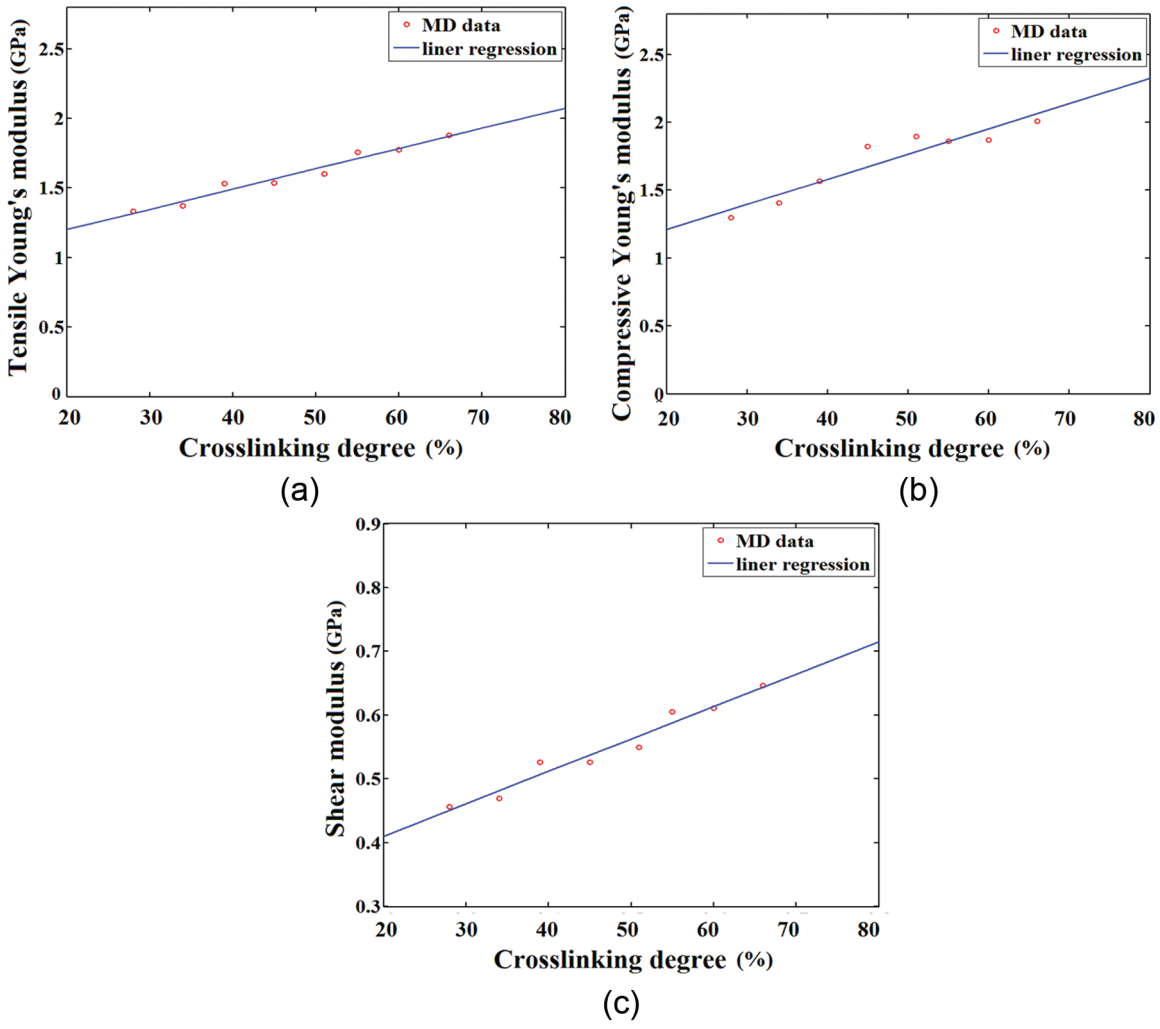


**Figure 7.** Relationship between cross-linking degree and (a) tensile modulus, (b) compressive modulus, and (c) shear modulus.

where $K$ is the bulk modulus, $V_0$ is the original volume of the RVE, and $\Delta p$ and $\Delta V$ are the change in pressure and change in RVE volume, respectively. From Young's modulus $E$ and the bulk modulus $K$ obtained from MD simulation, the shear modulus $G$ of the polymer system can be calculated using equation (4)

$$G = \frac{3KE}{9K - E} \tag{4}$$

Figure 7 shows the variation in elastic properties with cross-linking degree based on MD simulation results. These results provide the input for the spring–bead model and the network model at the microscale.

The moduli as a function of cross-linking degree $\theta$ are described in equations (5)–(7) using linear fitting functions

$$E_{tensile} = 0.01456\theta + 0.911 \tag{5}$$

$$E_{compressive} = 0.01857\theta + 0.839 \tag{6}$$

$$G_{shear} = 0.00507\theta + 0.309 \tag{7}$$

where $E_{tensile}$, $E_{compressive}$, and $G_{shear}$ are the tensile, compressive, and shear moduli, respectively; $\theta$ represents the cross-linking degree.

## Spring–bead-based network model at the microscale

### *Development of spring–bead-based network model*

The construction, evaluation, and the parametric studies of different network models are discussed in this section. Different kinds of network models, named according to the number of neighbor beads surrounding each bead (i.e. a 6 neighbor-based network model implies that each bead is connected with six neighbor beads using springs), are designed and compared. The network model, consisting of a series of beads and springs connected to neighboring beads, is used to represent larger cross-linked polymer chains and capture

**Table 2.** Configuration and evaluation of network models with different combination methods.

| Network model | Number of beads per 100 $\mu m^2$ | Number of springs per 100 $\mu m^2$ | Evaluation | Optimal isotropic index |
|---|---|---|---|---|
| 3 neighbors | 120 | 181 | Not stable | Not applicable |
| 4 neighbors | 156 | 313 | Not stable | Not applicable |
| 6 neighbors | 180 | 541 | Anisotropic | 1.1490 |
| 8 neighbors | 156 | 625 | Optimal model | 1.0008 |
| 12 neighbors | 180 | 1081 | Anisotropic | 1.1490 |

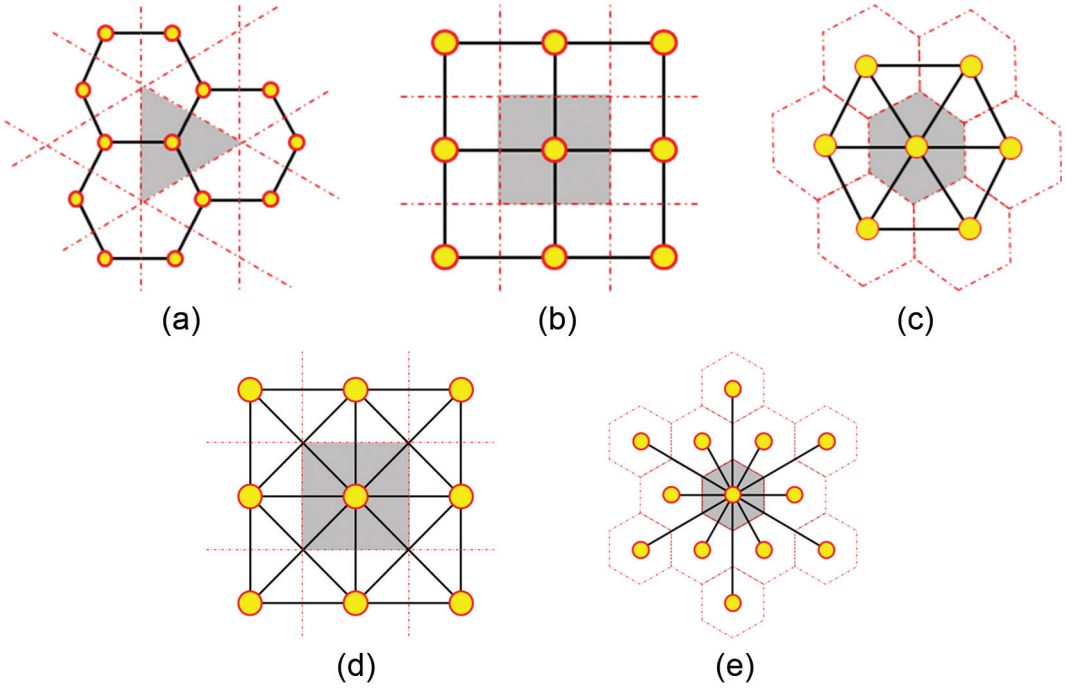


**Figure 8.** Different arrangements of spring–bead models to form a (a) 3 neighbor-based, (b) 4 neighbor-based, (c) 6 neighbor-based, (d) 8 neighbor-based, and (e) 12 neighbor-based network model.

the omnidirectional mechanical responses of the material. In addition, the network model serving as a simplified mechanical equivalent of MD simulations leads to significant reduction in computational cost and time compared to MD simulations.

Different combinations of spring–bead arrangements are studied to understand the mechanical response of the material. Several combination strategies (including 3, 4, 6, 8, and 12 neighbor-based connections) are shown in Figure 8. For example, in the 3 neighbor-based combination method (Figure 8(a)), one bead is linked with three neighbor beads. The bead located at the center of the gray area is used to represent the total mass of the corresponding area. The spring stiffness is equivalent to the load-carrying ability of the related bond cluster calculated from MD simulation. In the candidate network models, the spring length is defined as 0.8 μm; this value is also used as the lower bound if there is more than one kind of spring. The densities of springs and beads in the network models are listed in Table 2. It must be noted that complex network models with more neighbors will reduce simulation efficiency; therefore, network models with more than 12 neighbors are not considered in this study.

The candidate network models are listed in Figure 8. The optimal arrangement is the one that is capable of carrying tensile, compressive, and shear loads. Among the candidate combinations, the 3 and 4 neighbor-based models are not stable structures because they do not exhibit shear load-carrying capacity. Figure 9 illustrates the three remaining candidate network models (6, 8, and 12 neighbor-based arrangements). The optimized configuration is evaluated by how well a candidate model can represent the mechanical response at the microscale.

### *Parametric study of isotropic representation of network model*

The smart polymer is assumed to be homogeneous and isotropic at the macroscale. Therefore, the representation of isotropic property is considered to be an

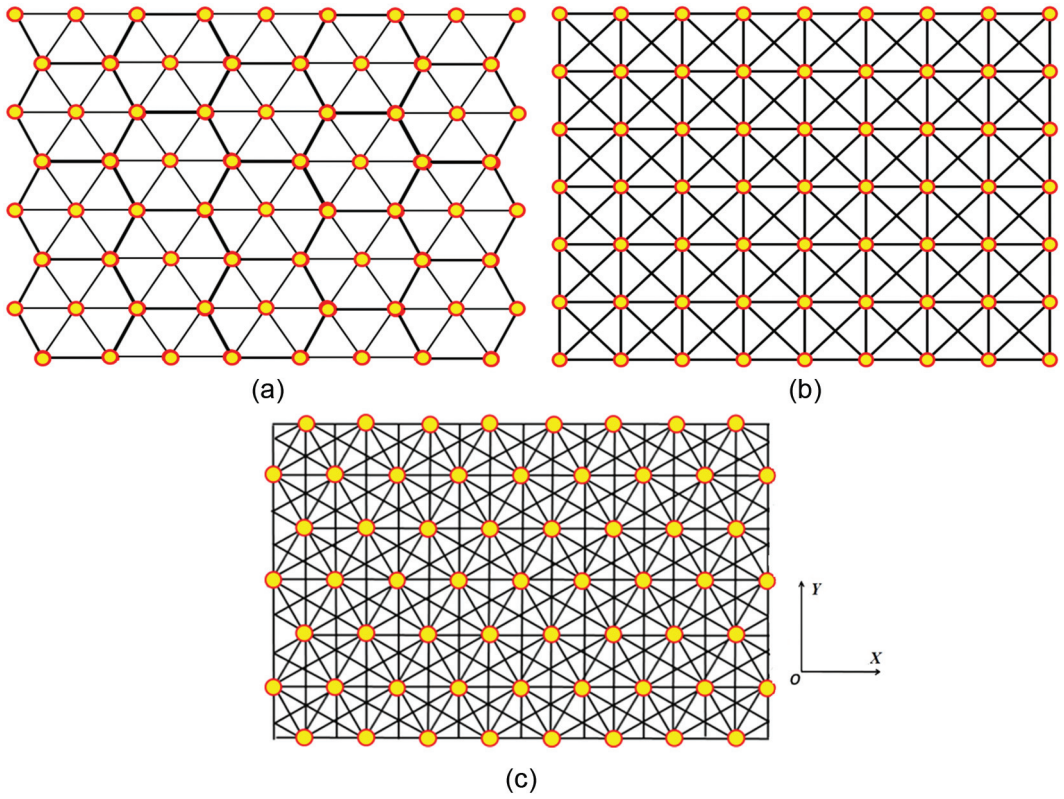


**Figure 9.** (a) Six neighbor based network model; (b) Eight neighbor based network model; (c) 12 neighbor based network model.

important criterion for evaluating the optimal network configuration. In all the network models proposed above, the springs are aligned along specific directions, depending on the type of the network configuration. For example, in the 8 neighbor-based network model (see Figure 9(b)), all the springs are at an angle of 0°, 45°, 90°, or 135°. Consequently, the mechanical response of all combined network models is dependent on orientations.

A 6 neighbor-based network model is set up with springs of uniform length, whereas the 8 and the 12 neighbor-based network models are made up of two types of springs (long and short). Since changes in the spring stiffness leads to the variations in mechanical response, the polymer material at different cross-linking degrees can be represented effectively by appropriately varying the $k_1$ (long spring) or $k_2$ (short spring) values. This feature provides the possibility of generating an equivalent isotropic network model using a specific ratio of spring stiffnesses. Additionally, an isotropy index is defined to describe the orientation dependence of mechanical response in the network model

$$I(\theta) = \frac{E_x}{E(\theta)} \tag{8}$$

In equation (8), $E_x$ represents Young's modulus in the principal direction ($x$-direction of the network model in Figure 9), $E(\theta)$ represents Young's modulus along an arbitrary direction at an angle $\theta$ with respect to the $x$-direction, and $I(\theta)$ is the isotropy index that shows the variation in material property along different directions. For a perfectly isotropic material, the isotropy index $I(\theta)$ is equal to 1. An isotropic index approaching unity is indicative of good isotropic material property representation.

The 6 neighbor-based network model fails to represent good isotropic property because it uses a single spring configuration; the average isotropy index of a 6 neighbor-based network model is 1.149 and the root mean square deviation (RMSD) between different directions is 7.45%. For the 8 and the 12 neighbor-based network models, a parametric approach was adopted to find the relation between the RMSD of mechanical responses in different directions and the stiffness ratio of long springs to short springs. From the simulation results, it can be observed that the average isotropy index is a continuously increasing function of stiffness ratio of springs. For the 8 neighbor-based network model, the RMSD is 0.04% when the stiffness ratio is 0.6002 (see Figure 10(a)). The maximum difference between mechanical responses along different directions is 0.08%. For the 12 neighbor-based configuration, the minimum isotropy index is 1.149 and the RMSD is 7.45% (same as 6 neighbor-based network model). Therefore, the 12 neighbor-based network

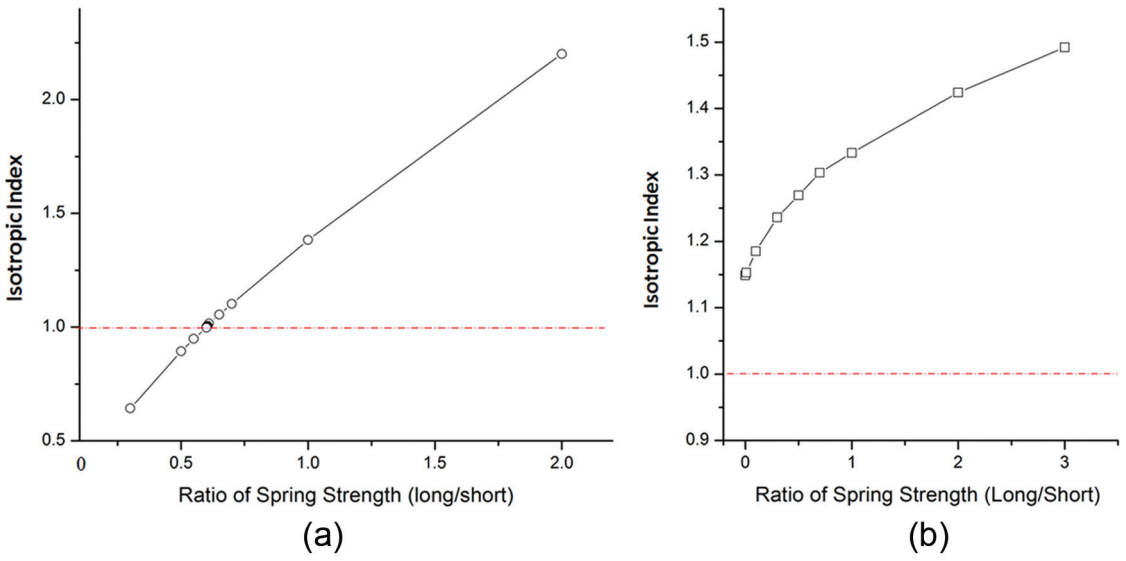


**Figure 10.** Isotropic representation of (a) 8 neighbor-based and (b) 12 neighbor-based network models corresponding to stiffness ratio of long spring to short spring.

model cannot adequately represent the isotropic property.

The evaluation of candidate network models is listed in Table 2. To summarize the results in this section, the 3 and the 4 neighbor-based network models cannot carry loads owing to their unstable structures, whereas the 6 and the 12 neighbor-based network models lack good isotropic representation capability. In addition, the 12 neighbor-based network model consists of a high number of springs and beads, which will increase simulation time and cost. The 8 neighbor-based network model is found to be the optimal one considering structural stability, representation of isotropic property, and computational efficiency. The 8 neighbor-based network model is equivalently isotropic when the ratio of long spring stiffness $k_2$ to short spring stiffness $k_1$ is given as 0.6002. It must be noted that a 2D spring–bead-based network model represents a polymer plate of unit thickness (1 μm). The spring stiffness will be redefined by multiplying a factor (ratio of material thickness to 1 μm) to represent different material thickness.

## *Bridging MD simulation and network model using mechanical equivalence optimization*

The network model integrated results from molecular level simulations to the microscale. Mechanical equivalence of the network model with the actual MD system also validates the approximation at the microscale. The next step is to determine the spring strengths that ensure minimal deviation of the mechanical response obtained from the network model and MD simulation. A multiobjective optimization technique is used to address this problem. The methodology also helps establish a relation between spring stiffness ($k_1$ or $k_2$) and the local cross-linking degree.

To obtain the relation between spring stiffness $k_1$ and the corresponding cross-linking degree $\theta$, a set of parametric studies are performed. First, a series of 8 neighbor-based network models are generated. The stiffness ratio of the springs is 0.6002 to ensure that the isotropic index is close to unity. The equivalent tensile, compressive, and shear strengths of network models are calculated for different spring stiffnesses. The simulation results and fitting curves indicate a linear relation between equivalent modulus of network model and spring stiffness $k_1$ (see Figure 11). The moduli (GPa) as functions of $k_1$ (N/m) are described by equations (9)–(11)

$$E'_{tensile} = 0.001494k_1 + 0.003286 \tag{9}$$

$$E'_{compressive} = 0.001476k_1 - 0.000210 \tag{10}$$

$$G'_{shear} = 0.000423k_1 + 0.000469 \tag{11}$$

The calculated value of all three moduli from the network model must match the corresponding values obtained from the MD simulation at a fixed cross-linking degree. A multiobjective optimization algorithm is formulated where the objective is to minimize the deviation for each loading condition

$$F_1(x) = \frac{f_T(k_1)}{E'_{tensile}} - 1 \tag{12}$$

$$F_2(x) = \frac{f_C(k_1)}{E'_{compressive}} - 1 \tag{13}$$

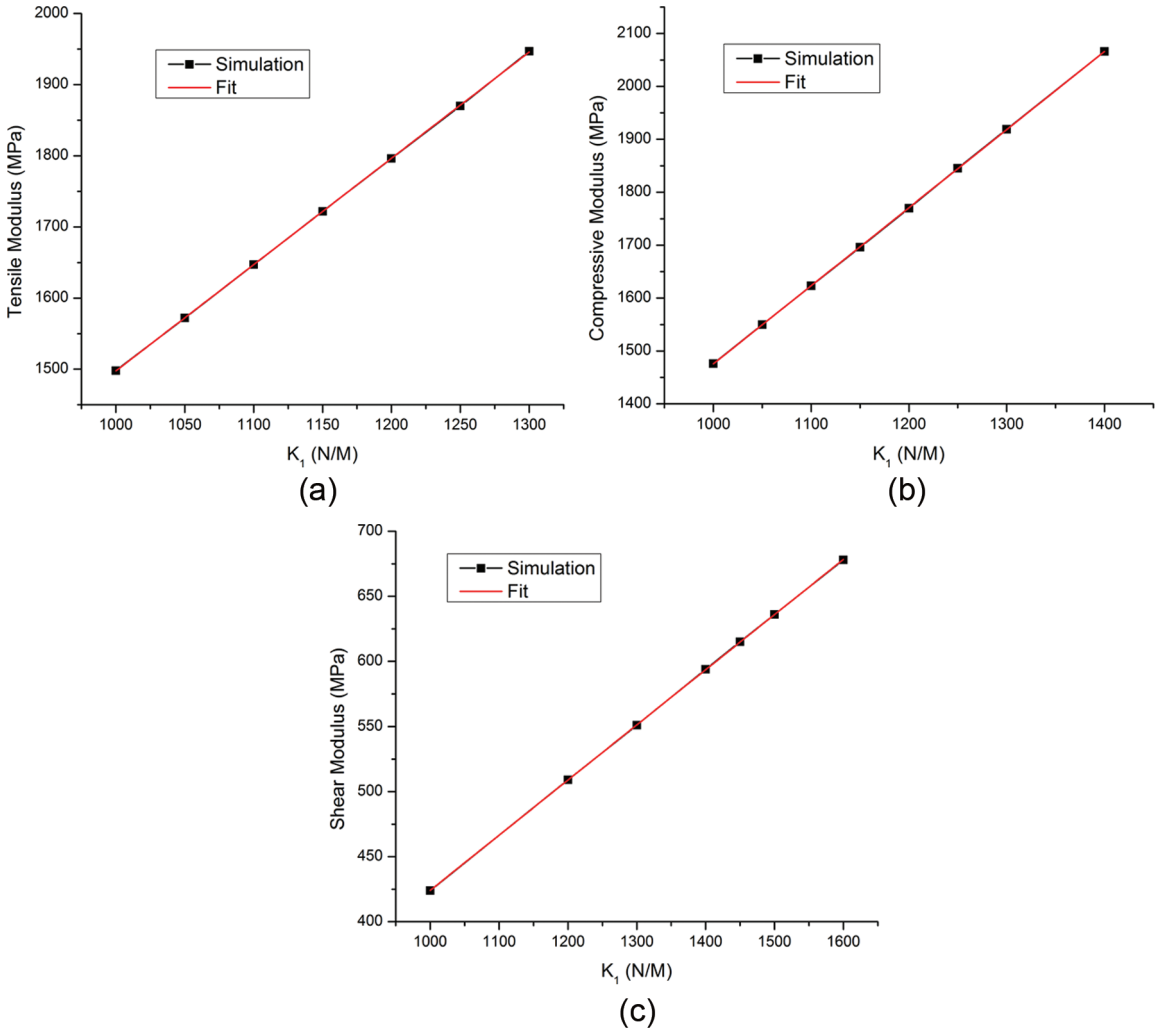


**Figure 11.** Fitting curves of modulus as a function of spring stiffness: (a) tensile modulus, (b) compressive modulus, and (c) shear modulus.

$$F_3(x) = \frac{f_G(k_1)}{G'_{shear}} - 1 \tag{14}$$

It must be noted that the objectives are competing as well as coupled; that is, the design variable, $k_1$, has a different degree of impact on each of the three objective functions, and the minimization of one objective could lead to an increase in the value of another objective. Therefore, a robust technique is required to determine the optimal spring stiffness at each cross-linking degree. The Kreisselmeier–Steinhauser (KS) function approach is used to solve the multiobjective optimization problem. Using the KS function, a composite envelope function is formulated to transform the original multiple objectives and constraints to a single unconstrained objective function (Chattopadhyay and McCarthy, 1991; Chattopadhyay and Seeley, 1994). Formulating the objective function in this approach involves the transformation of the original objective functions into reduced objective functions. The reduced objective functions are of the form

$$F^*(\boldsymbol{x}) = \frac{F_k(\boldsymbol{x})}{F_{k_o}} - 1 - g_{max} \leq 0 \quad k = 1, 2, \ldots, n_{obj} \tag{15}$$

where $F_{k0}$ corresponds to the value of $F_k$ calculated at the start of each iteration; "$g_{max}$" is the maximum value among all the constraints and remains constant throughout the iteration. The KS function combines the objectives and constraints ($n_{obj} + m = M$) to form the single objective function, described in equation (16)

$$\tilde{F}(\boldsymbol{x}) = g_{max} + \frac{1}{\rho} log \sum_{k=1}^{M} e^{\rho(g_k(x) - g_{max})} \tag{16}$$

The algorithm attempts to satisfy the constraints of the reduced objective function by maximizing $F_k$. The multiplier "$\rho$" is analogous to the draw-down parameter of penalty function formulations and controls the distance from the surface of the KS objective function to the surface of the maximum function value. A large value of "$\rho$" causes the KS function to closely follow

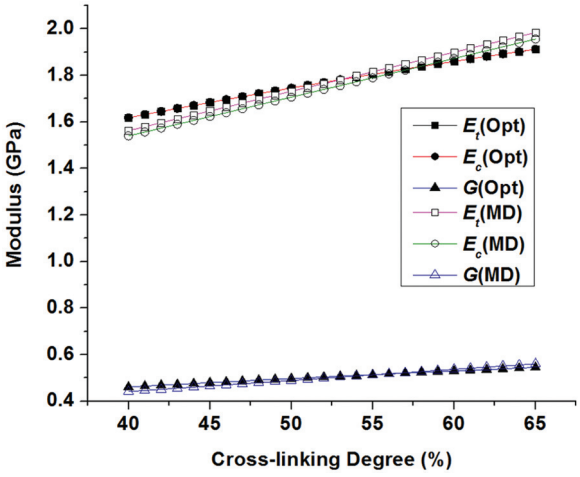


**Figure 12.** Comparison between MD simulation and optimization results.

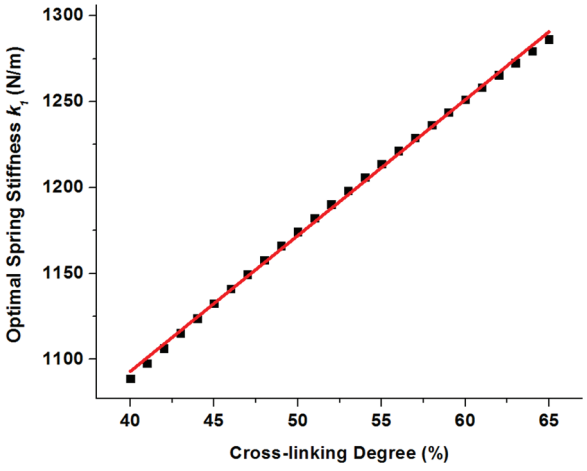


**Figure 13.** Linear fitting curve of spring stiffness based on optimization results.

the surface of the largest constraint function; a small value causes the inclusion of violated constraints to the KS function (Haftka and Gürdal, 1992).

Figure 12 compares the performance of the optimization algorithm with respect to the results from MD. The optimal $k_1$ value overestimates the values of the tensile and compressive moduli at lower cross-linking degrees. However, at the most likely cross-linking degree (~52.72%), the errors between the tensile and the compressive responses are quite balanced. The norm of the maximum constraint violation is within the specified tolerance of $1 \times 10^{-4}$. Figure 13 illustrates the variation in optimal spring stiffness with cross-linking degree. The relationship is a close linear approximation; this result is consistent with the inference from MD simulation that the tensile, compressive, and shear moduli vary linearly with cross-linking degree.

## Development of statistical network model

The relation between cross-linking degree and spring stiffness, obtained using the optimization technique, is used to construct the statistical network model. The springs with different stiffness are distributed stochastically in the representative network model (Figure 14(a)) to show the equivalent local variation in mechanical properties. The 8 μm × 8 μm area is divided into 100 (10 × 10) square grids. The numbers in the square grids in Figure 14(b) represent local cross-linking degrees of the corresponding subareas in network model in Figure 14(a). Table 3 shows the weight percentages of cross-linking degrees in the network model based on MD simulation. The spring–bead-based network model is implemented using the commercial FE software ABAQUS®. For the 8 neighbor-based network model with 8 μm × 8 μm area, there are 121 beads, 220 short springs, and 200 long springs.

**Table 3.** Weight percentages of different cross-linking degrees based on probability distribution results from MD simulation.

| Cross-linking degree (%) | Weight percentage (%) |
|---|---|
| 40–43 | 1 |
| 43–46 | 3 |
| 46–49 | 9 |
| 49–52 | 23 |
| 52–55 | 32 |
| 55–58 | 19 |
| 58–61 | 9 |
| 61–63 | 3 |
| 63–65 | 1 |

MD: molecular dynamics.

In the simulation, tensile and compressive representative loads are applied to the square network model. The simulation result of strain distribution under tensile load is shown in Figure 14(c). It can be observed that the deformation of the springs is dependent on its location. Based on the cross-linking degree distribution shown in Figure 14(b), there is an obvious relationship between local strain and cross-linking degree: high strain concentration (the upper hot color band in Figure 14(c)) occurs mostly where low cross-linking degree is observed (the upper blue rectangular area in Figure 14(b)), particularly where the cross-linking degree is under 50%. The results also show that the stochastic representative network model is capable of capturing heterogeneous properties of the material at the microscale. The high strain concentration sites are also related to potential local defects, which are influenced by both loading condition and local cross-linking degrees.

The mechanical response of a network model at the microscale is important for application of this model at

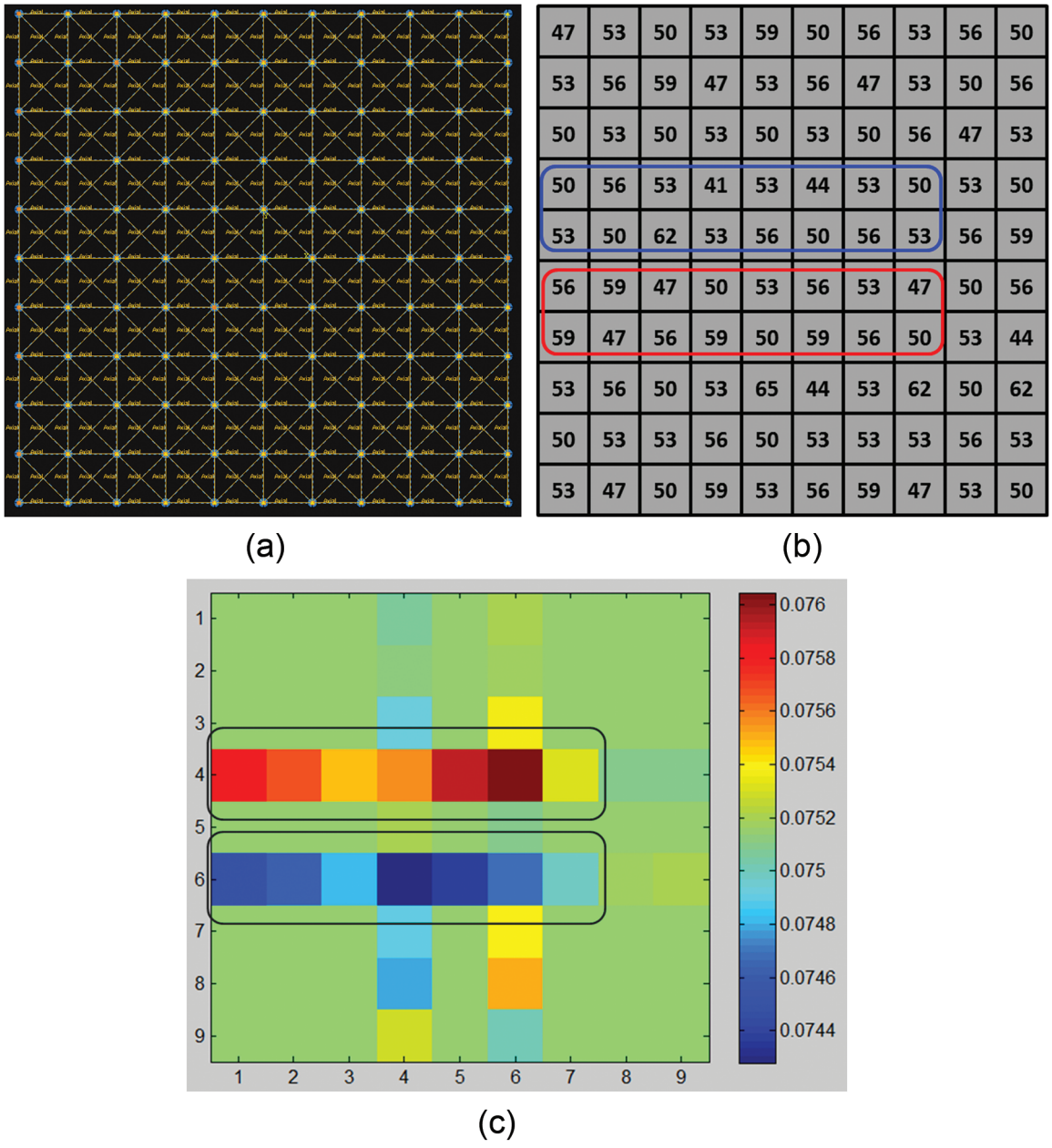


**Figure 14.** (a) Springs and beads' distribution, (b) cross-linking degree distribution, and (c) strain distribution in one statistical network model.

the structural scale. The statistical representative network models are constructed by assembling subareas (segmented and distributed in Figure 14(b)) whose spring stiffness is statistically sampled from a pool of probable characterization data based on MD simulation. Three stochastic representative network models were generated and the corresponding mechanical responses were compared between different network models to validate the reliability of the model, as shown in Table 4. The result shows that the errors in mechanical responses between different statistical representative network models are less than 1%, establishing the validity and robustness of the developed models.

**Table 4.** Simulation results from different network models.

| Material property | Model 1 | Model 2 | Model 3 |
|---|---|---|---|
| Young's modulus (GPa) | 1.77 | 1.76 | 1.77 |

A set of uniaxial compressive experiments were performed to determine Young's modulus of this smart material. An MTS Bionix 370.02 test frame (with the maximum loading capability 22.2 kN) was used to conduct the compressive tests. The comparison of results from the experiments and the simulations, shown in

**Table 5.** Comparison between experimental and simulation results.

| Material property | Experiment | Simulation | Error |
|---|---|---|---|
| Young's modulus | 1.82 GPa | 1.77 GPa | 2.7% |

Table 5, demonstrates that the error in Young's modulus prediction is 2.7%, making the spring–bead-based network model a good representation of the smart polymer material. It should be noted that the spring–bead-based network model improves the computational efficiency significantly. For a similar uniaxial tensile/compressive loading simulation, 20 h of runtime is required using MD simulation whereas a network model completes the simulation in 4 min. The simulation efficiency is thus improved by 300 times.

## Conclusion

A spring–bead-based network model was developed to represent the material properties of a polymeric material. At the nanoscale, the spring–bead model was developed to represent mechanical response and a mass of cluster bonds. MD simulation was implemented to provide necessary information to construct the model. At the microscale, a computationally efficient stochastic representative network model was developed; these models were implemented in a general-purpose FE solver to obtain the macroscale response. Parametric studies and multiobjective optimization were conducted to construct an optimal combination of an 8 neighbor-based network model and to determine the corresponding spring stiffness. The results show that the network model is capable of capturing both local heterogeneous property at the nanoscale and homogeneity at the microscale. The results representing the material properties obtained from the simulations and from the experiments are found to be in good agreement. The results from the network model provide insight into the relationship between low cross-linking degree and possible local damage zones. Compared to MD simulations, the spring–bead-based network model significantly improves the simulation efficiency while maintaining sufficient accuracy. The developed stochastic representative network model can successfully represent the material behavior of the polymeric material at relevant length scales.

### Declaration of Conflicting Interests

The authors declared no potential conflicts of interest with respect to the research, authorship, and/or publication of this article.

### Funding

The author(s) disclosed receipt of the following financial support for the research, authorship, and/or publication of this article: This work was partially supported by the Air Force Office of Scientific Research (grant no. FA9550-12-1-0331), and the program manager is Dr David Stargel. This work was also partially supported by the Office of Naval Research (grant no. N00014-14-1-0068), and the program manager is Dr William Nickerson.

### References

Bandyopadhyay A, Valavala PK, Clancy TC, et al. (2011) Molecular modeling of crosslinked epoxy polymers: the effect of crosslink density on thermomechanical properties. *Polymer* 52(11): 2445–2452.

Bawa P, Pillay V, Choonara YE, et al. (2009) Stimuli-responsive polymers and their applications in drug delivery. *Biomedical Materials* 4(2): 022001.

Borodin O, Bedrov D, Smith GD, et al. (2005) Multiscale modeling of viscoelastic properties of polymer nanocomposites. *Journal of Polymer Science Part B: Polymer Physics* 43(8): 1005–1013.

Buxton GA and Balazs AC (2002) Lattice spring model of filled polymers and nanocomposites. *The Journal of Chemical Physics* 117(16): 7649–7658.

Chang FK and Chang KY (1987) A progressive damage model for laminated composites containing stress concentrations. *Journal of Composite Materials* 21(9): 834–855.

Chattopadhyay A and McCarthy TR (1991) Multiobjective design optimization of helicopter rotor blades with multidisciplinary couplings. In: Hernandez S and Brebbia CA (eds) *Optimization of Structural Systems and Industrial Applications*. Computational Mechanics Publications, pp. 451–462.

Chattopadhyay A and Seeley CE (1994) A simulated annealing technique for multiobjective optimization of intelligent structures. *Smart Materials and Structures* 3(2): 98.

Cho SY, Kim JG and Chung CM (2008) A fluorescent crack sensor based on cyclobutane-containing crosslinked polymers of tricinnamates. *Sensors and Actuators B: Chemical* 134(2): 822–825.

Cho SY, Kim JG and Chung CM (2010) Photochemical crack healing in cinnamate-based polymers. *Journal of Nanoscience and Nanotechnology* 10(10): 6972–6976.

Chung CM, Roh YS, Cho SY, et al. (2004) Crack healing in polymeric materials via photochemical [2 + 2] cycloaddition. *Chemistry of Materials* 16(21): 3982–3984.

Fan HB and Yuen MM (2007) Material properties of the cross-linked epoxy resin compound predicted by molecular dynamics simulation. *Polymer* 48(7): 2174–2178.

Fermeglia M and Pricl S (2007) Multiscale modeling for polymer systems of industrial interest. *Progress in Organic Coatings* 58(2): 187–199.

Flory PJ and Rehner JJr (2004) Statistical mechanics of cross-linked polymer networks II. Swelling. *The Journal of Chemical Physics* 11(11): 521–526.

Gao L, Shillcock J and Lipowsky R (2007) Improved dissipative particle dynamics simulations of lipid bilayers. *The Journal of Chemical Physics* 126(1): 015101.

Ghosh S, Lee K and Moorthy S (1995) Multiple scale analysis of heterogeneous elastic structures using homogenization theory and Voronoi cell finite element method. *International Journal of Solids and Structures* 32(1): 27–62.

Gibson RF (2010) A review of recent research on mechanics of multifunctional composite materials and structures. *Composite Structures* 92(12): 2793–2810.

Haftka RT and Gürdal Z (1992) *Elements of Structural Optimization*, vol. 11. Springer Science & Business Media.

Hasan Z, Chattopadhyay A and Liu Y (2014) Multiscale approach to analysis of composite joints incorporating nanocomposites. *Journal of Aircraft* 52: 204–215.

Hossain D, Tschopp MA, Ward DK, et al. (2010) Molecular dynamics simulations of deformation mechanisms of amorphous polyethylene. *Polymer* 51(25): 6071–6083.

Iwata K (2003) Irreversible statistical mechanics of polymer chains. I. Fokker–Planck diffusion equation. *The Journal of Chemical Physics* 54(1): 12–26.

Krumova M, López D, Benavente R, et al. (2000) Effect of crosslinking on the mechanical and thermal properties of poly (vinyl alcohol). *Polymer* 41(26): 9265–9272.

Li C and Strachan A (2010) Molecular simulations of crosslinking process of thermosetting polymers. *Polymer* 51(25): 6058–6070.

Lin E, Niu L, Shi H, et al. (2012a) Molecular dynamics simulations of nano-scale interfacial friction characteristic for different tribopair systems. *Applied Surface Science* 258(6): 2022–2028.

Lin E, Niu L, Shi H, et al. (2012b) Molecular dynamics study on the nano-void growth and coalescence at grain boundary. *Science China: Physics, Mechanics & Astronomy* 55(1): 86–93.

Neerukatti R, Liu K, Kovvali N, et al. (2014) Fatigue life prediction using hybrid prognosis for structural health monitoring. *Journal of Aerospace Information Systems* 11(4): 211–232.

Peng T, Saxena A, Goebel K, et al. (2013) A novel Bayesian imaging method for probabilistic delamination detection of composite materials. *Smart Materials and Structures* 22(12): 125019.

Plimpton S, Crozier P and Thompson A (2007) LAMMPS-large-scale atomic/molecular massively parallel simulator. *Sandia National Laboratories*18.

Qiu Y and Park K (2001) Environment-sensitive hydrogels for drug delivery. *Advanced Drug Delivery Reviews* 53(3): 321–339.

Richter A, Paschew G, Klatt S, et al. (2008) Review on hydrogel based pH sensors and microsensors. *Sensors* 8(1): 561–581.

Rouse PEJr and Prince E (1953) A theory of the linear viscoelastic properties of dilute solutions of coiling polymers. *The Journal of Chemical Physics* 21(7): 1272–1280.

Schwarz US, Erdmann T and Bischofs IB (2006) Focal adhesions as mechanosensors: the two-spring model. *Biosystems* 83(2): 225–232.

Suzuki A, Ishii T and Maruyama Y (1996) Optical switching in polymer gels. *Journal of Applied Physics* 80(1): 131–136.

Tack JL and Ford DM (2008) Thermodynamic and mechanical properties of epoxy resin DGEBF crosslinked with DETDA by molecular dynamics. *Journal of Molecular Graphics and Modelling* 26(8): 1269–1275.

Tanaka T, Nishio I, Sun ST, et al. (1982) Collapse of gels in an electric field. *Science* 218(5471): 467–469.

Thostenson ET and Chou TW (2006) Carbon nanotube networks: sensing of distributed strain and damage for life prediction and self healing. *Advanced Materials* 18(21): 2837–2841.

Tomar V, Zhai J and Zhou M (2004) Bounds for element size in a variable stiffness cohesive finite element model. *International Journal for Numerical Methods in Engineering* 61(11): 1894–1920.

Underhill PT and Doyle PS (2005) Development of bead-spring polymer models using the constant extension ensemble. *Journal of Rheology* 49(5): 963–987.

Varshney V, Patnaik SS, Roy AK, et al. (2008) A molecular dynamics study of epoxy based networks: cross-linking procedure and prediction of molecular and material properties. *Macromolecules* 41(18): 6837–6842.

Wu DY, Meure S and Solomon D (2008) Self-healing polymeric materials: a review of recent developments. *Progress in Polymer Science* 33(5): 479–522.

Yarovsky I and Evans E (2002) Computer simulation of structure and properties of crosslinked polymers: application to epoxy resins. *Polymer* 43(3): 963–969.

Yu S, Yang S and Cho M (2009) Multi-scale modeling of cross-linked epoxy nanocomposites. *Polymer* 50(3): 945–952.

Zeng Q, Yu A and Lu G (2008) Multiscale modeling and simulation of polymer nanocomposites. *Progress in Polymer Science* 33(2): 191–269.